batteries

MDPI

Article

Comprehensive Study of the Gas Volume and Composition Produced by Different 3–230 Ah Lithium Iron Phosphate (LFP) Cells Failed Using External Heat, Overcharge and Nail Penetration Under Air and Inert Atmospheres

Gemma E. Howard *, Jonathan E. H. Buston, Jason Gill, Steven L. Goddard, Jack W. Mellor and Philip A. P. Reeve

HSE Science and Research Centre, Harpur Hill, Buxton Derbyshire SK17 9JN, UK; jonathan.buston@hse.gov.uk (J.E.H.B.)
* Correspondence: gemma.howard@hse.gov.uk

Abstract

This paper reports on the failure of cells with lithium iron phosphate (LFP) chemistry tested under a range of conditions to understand their effect on the volume and composition of gas generated. Cells of the following formats, 26,650, pouch, and prismatic, and capacities ranging from 3 to 230 Ah, were subjected to external heat, overcharge, and nail penetration tests. Gas volume was calculated, and the following gases analysed: H_2, CO_2, CO, CH_4, C_2H_4, C_2H_6, C_3H_6, and C_3H_8. Cells that failed via external heating under inert conditions (N_2 or Ar atmosphere) at 100% state of charge (SoC) typically generated 0.7 L/Ah of gas; overcharged cells, 0.11–0.68 L/Ah; and nail penetration between 0.3 and 0.5 L/Ah. In general, for all test configurations, regardless of atmosphere, the total gas volume contained a 40% concentration of H_2, 15% of CO_2, and the remaining gas consisted of varying concentrations of CO and flammable hydrocarbons. This demonstrates that despite differences in gas volume, the failure gas composition of LFP cells remains similar.

Keywords: Li-ion; lithium iron phosphate (LFP); gas analysis; gas volume; 22,650; pouch cell; prismatic cell; external heat; overcharge; nail penetration

Academic Editor: Xianglin Li

Received: 13 May 2025
Revised: 8 July 2025
Accepted: 11 July 2025
Published: 16 July 2025

Citation: Howard, G.E.; Buston, J.E.H.; Gill, J.; Goddard, S.L.; Mellor, J.W.; Reeve, P.A.P. Comprehensive Study of the Gas Volume and Composition Produced by Different 3–230 Ah Lithium Iron Phosphate (LFP) Cells Failed Using External Heat, Overcharge and Nail Penetration Under Air and Inert Atmospheres. *Batteries* **2025**, *11*, 267. https://doi.org/10.3390/batteries11070267

1. Introduction

Lithium-ion batteries (LiBs) are currently the standard choice for consumer electronics, electric vehicles (EVs), and portable equipment for commercial and residential use. The global campaign to achieve Net Zero has driven the popularity of alternative strategies, including the implementation of LiBs to electrify transport and energy storage applications [1]. In particular, cells with lithium iron phosphate chemistry (LFP) are being used for these applications, especially in EV manufacture by companies including BYD, Tesla, and Ford. This is due to LFP cells having cost benefits and perceived safety advantages over Ni-based cells [2–4].

In general, cells exposed to conditions outside their normal operating range risk failure. During failure, cells can enter thermal runaway (TR), where internal heat production exceeds the rate at which heat is able to dissipate to the surrounding environment, preventing cell cooling. The heating of the cell causes thermal decomposition of the electrolyte and generates gas [5]. Compared to Ni-based cells, LFP cells typically require higher temperatures to enter TR, and the failure gases typically do not self-ignite [6,7]. Ignition of gas from LFP

cells from an external ignition source may be possible, depending on gas composition and concentration, which can result in fire [8]. The safety implications highlight the importance of understanding how factors, including cell manufacturer, capacity, state of charge (SoC), and abuse method, affect gas volume and composition.

Published data for generated gas volumes during failure are available for smaller capacity 18,650 and 26,650 LFP cells (1.1–5 Ah) under both air and inert atmospheres. All gas volumes have been converted to standard atmospheric temperature and pressure (SATP) to allow easier comparison. Cells that were reported to fail by external heating at 100% SoC under an air atmosphere generated 0.9–1.5 L/Ah, and those that failed under inert conditions generated 0.5–1.4 L/Ah [6,9,10]. The minimal difference in gas volume between the different atmospheres may be due to the typical failure mechanism of LFP cells, where they do not typically ignite. The arrangement of cells in a cell block was also reported not to appear to significantly affect the gas volume produced compared to single cell tests in either atmosphere. The failure of two- and three-cell blocks under air produced 0.9 and 1.2 L/Ah, respectively, and a seven-cell block under N_2 was reported to generate 1.4 L/Ah [10–12]. There is less data available for larger capacity LFP cells; however, 23, 196, and 266 Ah prismatic cells at 100% SoC were reported to generate 0.5 L/Ah when externally heated to failure under inert atmospheres [13–15].

A study considering the effect of SoC on gas volume production found that under air atmospheres above 50% SoC, the volume of gas generated was 0.6–1.2 L/Ah; however, at 25% SoC, nearly double the volume of gas, 2.3 L/Ah, was generated [9]. Similar results were also observed in two of the cell types tested by Yang under an Ar atmosphere. Above 50% SoC, the gas volume generated by one cell type was 1.2–1.6 L/Ah, and 3.1 L/Ah at 25% SoC, and the second cell type, 1.3–1.5 L/Ah, and 2.9 L/Ah at 25% SoC [16]. For the other two cell types, tested gas volumes generated were between 1.0 and 1.6 L/Ah across all SoCs [12].

Gas volume data for cells that failed by overcharging in an air atmosphere typically generated much less gas than similar cells that failed by external heat. Yang et. al. tested a range of 18,650, 26,650, and 26,700 LFP cells with capacities ranging from 1.1 to 4.0 Ah. In general, cells generated 0.2–0.6 L/Ah, with a single cell generating nearly double the volume of gas, 1.1 L/Ah [16]. Another overcharge test by Fernandes et. al. also generated gas volumes within a similar range at 0.5 L/Ah [17]. Gas volume generation for nail penetration tests at 100% SoC varied greatly between atmospheres for the same cell. The cell that failed under an air atmosphere generated 0.01 L/Ah compared to 1.5 L/Ah for that which failed under N_2 [18].

Gas data indicates that LFP cells generate higher concentrations of H_2 compared to Ni-based cells, which can affect the likelihood of the gas igniting in the presence of an ignition source [10]. Data suggests that when LFP cells fail at a 100% SoC, most gas generated is comprised of H_2 and CO_2, regardless of whether the cell failed under air or inert conditions. Golubkov found that LFP cells that failed at 100% SoC via external heat under an Ar atmosphere generated a CO_2 concentration of 53% and an H_2 concentration of 31% [6]. Even higher concentrations were documented by Said in a N_2 atmosphere with H_2 contributing 81% to the total gas volume, followed by CO_2 at 11.1% [19].

In higher capacity LFP cells, gas composition was seen to be similar for tests on lower capacity cells. H_2 was found in the highest concentrations in the failure gas of 196 and 266 Ah cells, contributing between 42 and 54%, followed by CO_2 (24–26%) [14,15]. Other gases reportedly detected in the gas samples collected included CO, CH_4, and other hydrocarbons.

The effect of SoC on gas concentrations has also been documented. Peng found that both the concentration of CO and CO_2 increased with cell SoC, for cells tested using an

air atmosphere. However, when testing under an inert atmosphere, Golubkov found that the increase in SoC led to a decrease in CO_2 concentration and an increase in CO concentration [9,20]. The concentration of H_2 was also found to increase with SoC, and the presence of CH_4, C_2H_4, and C_3H_6 was also detected; however, SoC had a seemingly minimal effect on concentration levels of these gases [12].

Similar compositions have been observed in the gas generated by cells that failed due to overcharging. The presence of CO_2 and CO was detected in testing of two different cell types; in addition to these, H_2 was observed by Wang and C_2H_4 by Fernandes [17,18]. Overcharging of eight different cell types by Yang found that the main gas constituents were H_2 and CO_2, similar to those observed in external heat tests [16]. The presence of CO and smaller hydrocarbons was also identified.

Data for nail penetration was limited. Wang recorded a small amount of gas released from cells that failed via nail penetration; however, this was not sufficient to identify or quantify any gaseous species [18].

The data above typically exhibits results for external heat tests on lower capacity LFP cells, specifically at <5 Ah. Often, only one data point is reported, and therefore does not account for any variation in the failure of the same cell. There is also a range of different experimental techniques used, making it difficult to compare between tests.

In this paper, we present for the first time a single dataset on gas volumes and compositions. Results were obtained through the same experimental method for LFP cells, ranging from small capacity cylindrical cells (2.5–3.3 Ah) to much larger capacity pouch and prismatic formats (22–230 Ah). An insight was provided into the effect that cell capacity, format, and cell failure method can have on gas volume and composition generated by failed cells. When possible, tests have been repeated to provide more than one data point to understand the range of results obtained under the same test conditions. By providing this data, we seek to give a validated first estimate for the volume and composition of gas generated by the failure of a variety of LFP cell formats, capacities, and manufacturers. Demonstration of these differences highlights the importance of testing the individual cell type to be used in the application by the operator, to understand the outcomes of a potential cell failure.

2. Materials and Methods

The test series aimed to understand the gas volume and composition produced during the failure of a cell with LFP chemistry. The project was split into the following four key sections, each with an individual aim and method:

1. Comparison of external heat tests on 2.5–3.3 Ah 26,650 cells from different manufacturers.
2. Effect of SoC and abuse method on a 3 Ah 26,650 cell.
3. Comparison of external heat and overcharge on pouch and prismatic higher capacity (22–230 Ah) cells.
4. Open-field nail penetration tests on pouch and prismatic cells.

All tests in Sections 1–3 were performed inside a bespoke pressure vessel, with the same methodology (Sections 2.1–2.3) used to calculate the gas volume and perform gas composition analysis. Further details on the pressure vessel set-up and calculations are outlined in the following sections.

2.1. Pressure Vessel Set-Up

All tests within the experimental series were performed inside a 47 L pressure vessel rated to 10 bar at 200 °C, contained within a blast chamber and remotely operated. Temperature data was collected using type-N (accuracy ± 2.2 °C) thermocouples placed above the cell, inside the pressure vessel (ambient temperature), and on the cell's surface (cell

temperature). Pressure data measurements were taken using a 0–2 bar pressure transducer for lower capacity cells and 0–7 bar for higher capacity cells. The pressure transducer was placed on the back wall of the pressure vessel, and data measurements were taken at a rate of 10 ms. Depending on the test requirements, the pressure vessel had either an air or inert (N_2 or Ar) atmosphere. To achieve the inert atmosphere, the vessel was purged seven times, bringing the O_2 concentration to >0.05%. When required, a gas sample was collected via a sampling vent to a 5 L Tedlar bag once the vessel temperature had returned to ambient temperature.

2.2. Gas Volume Calculations

The volume of gas generated during cell failure was calculated using the ideal gas law. During the test, the ambient temperature and pressure were recorded and used in the gas volume calculations. By calculating and normalising the initial moles, the additional gas volume could be attributed to the cell failure. The number of moles was subsequently used to calculate the final gas volume. The values were standardised to give the gas volume at standard atmosphere temperature and pressure (SATP) (298 K, 101,325 Pa), allowing for easier comparison between tests [21–23].

2.3. Gas Composition Analysis

The composition of gas collected after testing was analysed by mass spectrometry using a Hiden Analytical™ HPR-20 quadrupole mass spectrometer with a heated capillary tube. Raw data was converted into % volume by subtracting the contribution of overlapping fragment ions and converting them using the instrument's relative sensitivity factors for the target gas. A background subtract was applied to the data prior to conversion. Data was collected over a 0–150 m/z mass range and specifically quantified for the following target gases: H_2, CO_2, CO, C_2H_6, C_2H_4, C_3H_6, C_3H_8, and CH_4, based on the literature review. If any other gases were present in the samples, it was assumed to be at very low concentrations, therefore negligible [11]. Only permanent gas was included in the final analysis results, therefore excluding possible vapour concentration. Gas analysis was carried out on the same day as testing. Further details for the gas composition analysis calculations have previously been reported [21]. Although we present gas composition data, we do not explore the mechanisms behind this formation, which has been previously reported and assessed to be due to decomposition reactions of the solid electrolyte interphase (SEI) layer or electrolyte [15].

2.4. 26650 Cell Characterisation

The first set of tests compared the gas volume and composition generated when four 26,650 cells, from different manufacturers, failed by external heating. Each cell type was referred to as Cell A, B, C, or D, and the details for each cell are summarised in Table 1.

Table 1. Details for Cell A, B, C, and D, including format, weight, capacities, and internal resistance (IR). All values are given as an average of three cells.

Cell ID	Cell A	Cell B	Cell C	Cell D
Format	Cylindrical, 26,650			
Weight (g)	83	86	84	87
Rated Capacity (Ah)	3.0	3.3	2.5	3.0
Average Actual Capacity (Ah)	2.9	3.5	2.4	2.9
Maximum Rated Continuous Discharge Rate (A)	15	5	50	9
IR (mΩ)	2.1	6.6	3.2	1.0

Prior to testing, each of the four cell types was charged (constant current constant voltage, CCCV) to 100% (3.65 V) and discharged at a rate of 1.5 A to 2.5 V, with a rest of five minutes between each step. The cycle was repeated a total of three times, and the capacity at the end of the charge cycle was used to calculate the actual cell capacity. The cells were then discharged to a final capacity of 1 Ah, as defined in the charging routine. Cells were charged using an MTI charger (BST 8 5A CST). Once at a 1 Ah capacity, internal resistance (IR) and electrical impedance spectroscopy (EIS) measurements were taken for each cell type. Internal resistance measurements were performed using 1 kHz (Applent AT526).

Alternating current internal resistance (ACIR). EIS measurements were taken using a Gamry Instruments Interface 1000E potentiostat. The initial frequency was set to 1000 Hz, and the final frequency was 0.005 Hz. The AC voltage used was 10 mV rms with an estimated impedance (Z) of 0.1 Ω. The Bode plot and Nyquist graph are plotted in Figure 1.

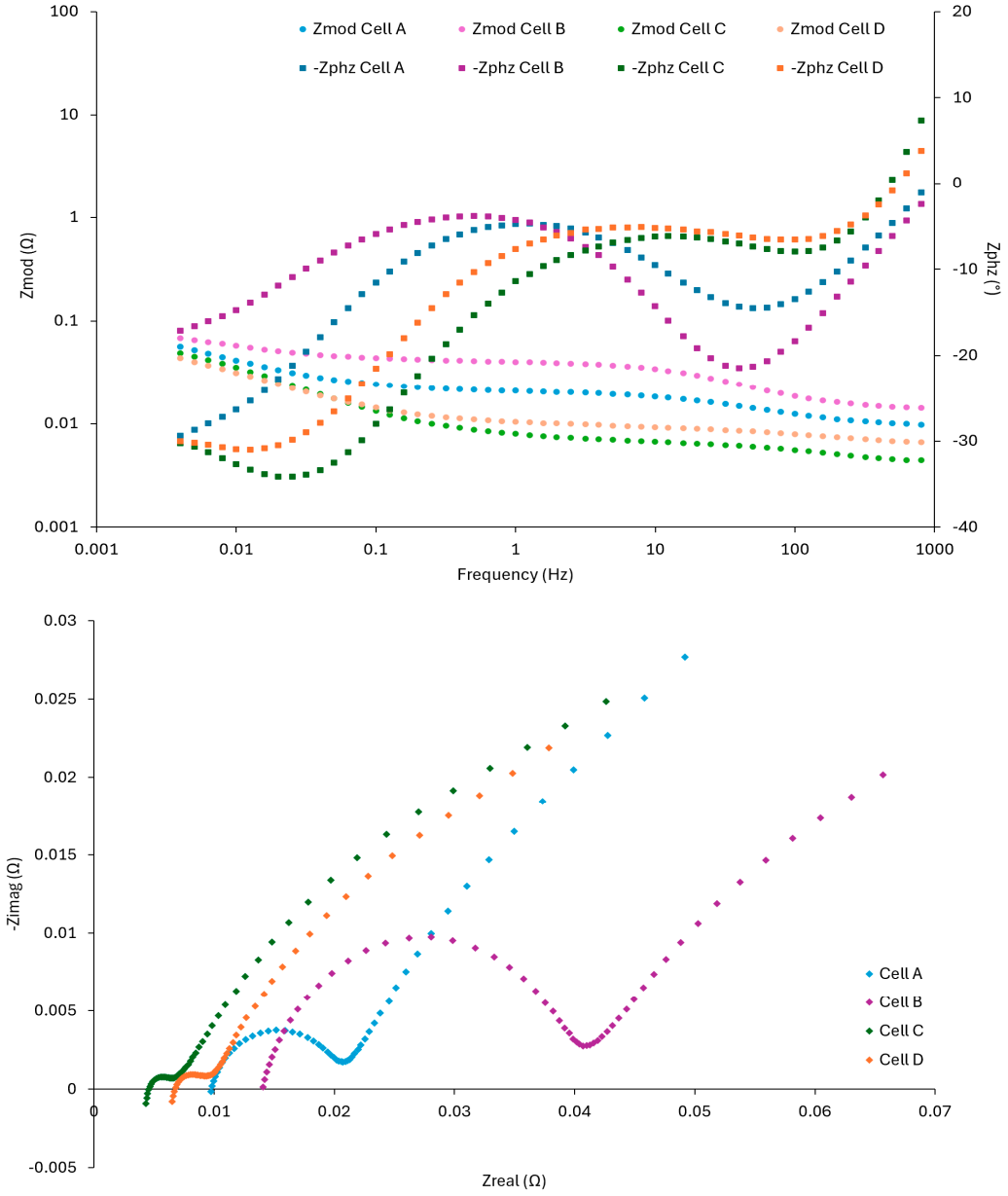

Figure 1. Bode (**top**) and Nyquist (**bottom**) plots for a single representative 'Cell A' (green), 'Cell B' (blue), 'Cell C' (red), 'Cell D' (pink). EIS was performed after three charge cycles to a 100% SoC and final discharge step to a capacity of 1 Ah.

2.4.1. The 26,650 Cells External Heat Test Set-Up

Each of the 26,650 cells failed via the application of external heat at a 100% SoC. A 3 × 2″-10P adhesive heater (Omega, KHLVA-203/10P) was attached to the cell's surface and supplied with an electrical power of 30 W, heating the cell until failure (Figure 2a). Two tests under inert conditions and one under air were performed for each cell type. Cell D was also tested at 33 and 67% SoC under inert conditions and 50% SoC under air.

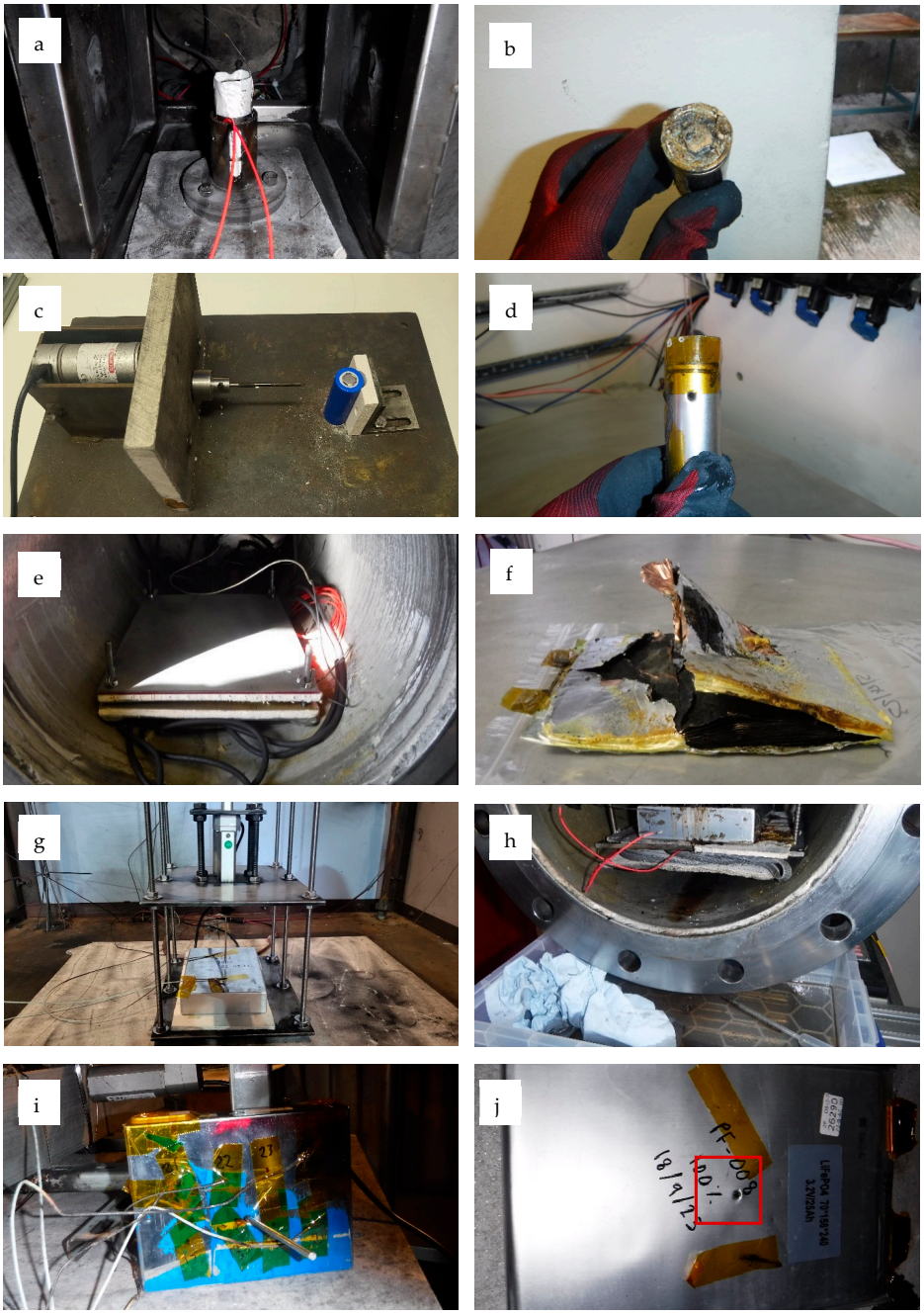

Figure 2. Before and after pictures for the following tests: (**a**) 'Cell D' external heat pressure vessel before, (**b**) 'Cell D' external heat after, (**c**) 'Cell D' nail penetration pressure vessel before, (**d**) 'Cell D' nail penetration after, (**e**) 25 Ah pouch (Cell F) cell external heat before, (**f**) 25 Ah pouch (Cell F) after external heat test (**g**) 105 Ah prismatic (Cell J) cell nail penetration test before, (**h**) 105 Ah prismatic (Cell J) cell external heat electrolyte in bottom of pressure vessel, (**i**) 50 Ah prismatic (Cell H) cell nail penetration open-field after, and (**j**) 25 Ah pouch (Cell F) cell nail penetration open-field after, puncture hole highlighted by red box.

2.4.2. The 26,650 Nail Penetration Test Set-Up

Nail penetration tests were also performed on Cell D at 100% SoC under an inert atmosphere. Mechanical failure was achieved using a custom rig containing an actuator with a nail held perpendicular to the cell's centre (Figure 2c). The nail had a 3 mm diameter with a point angle of 30 degrees and travelled at a speed of approximately 0.1 m/s.

2.5. Higher Capacity (22–230 Ah) Pouch and Prismatic Cell Tests

A number of external heat and/or overcharge tests were performed on seven different types of LFP pouch and prismatic cells, ranging in capacity from 22 to 230 Ah. Prior to testing, cells were characterised to collect cell weights and IR, where possible, using ACIR at 1 kHz. IR measurements were taken from cells as they were removed from the box, at approximately 30% SoC. The cell details are summarised in Table 2.

Table 2. Higher capacity LFP cells format, capacity, model, and manufacturer details. The weight is given as an average of 3 cells. The internal resistance (IR) of a single cell of each type as new, approximately 30% SoC is also given. (* The IR was not measured for 'Cell I', 'Cell J', or 'Cell K').

Cell ID	Format	Nominal Capacity (Ah)	Measured Capacity (Ah)	Weight (g)	IR (Ω)	Dimensions (mm)
E	Prismatic	22	21	636	2.81	145 × 130 × 15
F	Pouch	25	25	510	1.07	150 × 240 × 60
G	Prismatic	32	33	745	1.35	150 × 90 × 25
H	Prismatic	50	53	987	0.71	145 × 115 × 25
I	Prismatic	50	N/A	1404	*	135 × 180 × 30
J	Prismatic	105	109	1987	*	130 × 195 × 35
K	Prismatic	230	242	4158	*	170 × 205 × 50

2.5.1. Higher Capacity Cells External Heat Test Set-Up

For the higher capacity cells, which failed using external heat, a heater was attached to 1 mm stainless steel plates placed on either side of the cell. These were insulated by 6 mm calcium silicate fireboard, and 3 mm stainless steel plates were then placed on either side. These stainless-steel sheets were bolted together in all four corners to prevent cell swelling during the test (Figure 2e). Fireboard was placed between the cell and the pressure vessel's inside walls to prevent flame impingement. All cells tested were charged to a 100% SoC and tested under an Ar atmosphere. Gas samples were collected and analysed for all tests unless stated otherwise. The exact size of the heater and power supplied varied between tests, due to heater availability. The exact details of the heater and power supplied for each test are detailed in the supplementary data. Studies by Chen suggest that the heater power did not affect gas composition [24]. Overall, four tests were performed on 'Cell F', three on 'Cell H', and three on 'Cell J'.

2.5.2. Higher Capacity Cells Overcharge Test Set-Up

As described in previous tests, these cells were placed inside a pressure vessel with either an air or an Ar atmosphere. The rate at which the cell was charged varied between tests, due to the maximum current able to be supplied by the power supply. The starting SoC also varied between tests. The test set-up details, including starting SoC and charging current, are summarised in Table 3.

Table 3. Overcharge test set-up summary including pressure vessel atmosphere, number of tests, starting state of charge (SoC), and overcharge rate.

Cell ID	Atmosphere	Number of Tests	Starting SoC (%)	Overcharge Current (A)
Cell E	Air	2	75	11 (0.5 C)
Cell E	Ar	2	75	11 (0.5 C)
Cell G	Ar	2	75	16 (0.5 C)
Cell I	Ar	1	75	25 (0.5 C)
Cell J	Ar	2	75	26 (0.25 C)
Cell K	Ar	2	100	30 (pressure vessel current limit)

2.5.3. Higher Capacity Cells Open-Field Nail Penetration Tests

Open-field nail penetration tests were performed on the 50 Ah prismatic (Cell H), 105 Ah prismatic (Cell J), and 25 Ah pouch (Cell F) cells, all at a 100% SoC (Figure 2g). Testing was performed within a battery abuse test chamber using a custom-built nail penetration rig. This rig was used to pierce to cell's centre at a depth of half the cell's height. A nail of 3–4 mm with a 30-degree point angle was set to travel at 0.1 m/s. Type-K thermocouples were attached to the surface of the cell and were used to record temperature changes during the test. The aim of these experiments was to characterise the failure events before using the pressure vessel and determine if useful data could be collected. However, the cells did not enter TR, have a significant temperature rise, or generate any visible gas/smoke; therefore, no tests were performed inside the pressure vessel.

A series of images of the various test set-ups and cells after failure can be found in Figure 2.

3. Results and Discussion

3.1. The 26,650 Cells External Heat Tests

Four different LFP 26,650 cells are compared under a range of conditions. Cells A–D failed at 100% SoC under air and inert conditions. All gas volume and composition results are summarised in Table 4.

Table 4. Gas volumes generated by Cells A–D during an external heat test at a 100% state of charge (SoC). (Note: All N_2 tests and Cell A air tests are an average of 2 results, and Cells B and C air tests are from a single data point).

Cell ID	Atmosphere	Capacity (Ah)	Max. Temps. (°C)	Average Net Gas Volume (L)	Average Gas Volume (L/Ah)	Average Gas Composition							
						H_2 (%)	CO (%)	CO_2 (%)	CH_4 (%)	C_2H_6 (%)	C_2H_4 (%)	C_3H_8 (%)	C_3H_6 (%)
A	N_2	3.0	368–339	2.0	0.65	42.7	0.0	11.3	20.3	7.3	6.1	7.8	4.5
A	Air	3.0	280	2.4	0.80	42.2	0.7	15.5	14.7	7.3	5.7	8.9	4.9
B	N_2	3.3	226–315	1.8	0.50	47.6	1.8	19.1	10.4	2.4	4.9	10.3	3.6
B	Air	3.3	270	1.1	0.33	36.9	0.0	30.8	13.2	0.7	4.2	11.5	2.7
C	N_2	2.5	245–369	2.1	0.82	27.0	16.8	28.6	17.6	2.3	1.5	5.1	1.3
C	Air	2.5	304	1.3	0.52	39.1	4.1	25.1	12.8	2.6	6.1	6.9	3.2
D	Ar	3.0	318–409	3.1	1.03	12.9	8.2	16.8	14.5	3.2	4.4	10.7	1.7
D	Air	3.0	327–348	2.5	0.83	-	-	-	-	-	-	-	-

Although the cells used during the external heat tests contained the same LFP chemistry and format, there was a wide variation in gas composition between the test atmosphere and cell types. The electrolyte solvent composition used in cell manufacture could be a contributing factor to the observed differences. The failure events, such as resulting temperatures, electrolyte decomposition mechanism, and combustion rate, also affect the final gas composition. Whilst indicative gas volumes and approximate gas volumes can be derived,

this shows the importance of conducting experimental studies when collecting data to be used in understanding safety implications.

For Cell A, the gas volumes were similar across the test series, despite changing the atmosphere. The comparison open-field tests demonstrated no visible signs of flames or smoke, which suggested combustion reactions did not occur. Therefore, the gas detected is likely to be the result of electrolyte solvent decomposition during the failure event, which led to a higher percentage of H_2 in the final ratio.

Despite Cell A and Cell D having the same capacity, Cell D generated more gas in the inert atmosphere than Cell A, 3.1 L vs. 2.0 L, respectively. The gas analysis comparison showed very similar percentage volumes for H_2 and the small hydrocarbons; however, the main differences were the volumes of CO_2 and CO. For Cell D, a higher proportion of CO_2 was detected alongside a small percentage of CO. The presence of CO was not detected in Cell A with an increased percentage volume of CH_4 present, 20.3% compared with 14.5% for Cell D. They did, however, produce similar gas volumes in air. Unfortunately, gas analysis samples were not taken for Cell D in air, so this comparison cannot be made.

Cell B and Cell C generated smaller gas volumes in an air atmosphere and showed differences in gas composition. Cell B generated a larger proportion of H_2 in the N_2 atmosphere, accounting for almost half of the percentage volume, 47.6% compared to 36.9% in air. The lack of CO in air and a high proportion of CO_2 are likely due to the decomposition of electrolytes. The composition of small hydrocarbons did not vary between the atmospheres for Cell B, indicating their formation is not dependent on O_2 concentration and combustion reactions.

Gas analysis results for Cell C have the opposite trend to Cell B, generating less H_2 in the N_2 atmosphere, 27.0% compared to 39.1% in the air atmosphere. There was also a higher proportion of CO, CO_2, and CH_4 in the gas sample taken from the N_2 atmosphere. The percentage volumes for the hydrocarbons were similar between atmospheres except for C_2H_4, which was approximately four times higher in air than N_2, 6.1% and 1.5%, respectively.

Overall results indicate that regardless of the atmosphere in which the cell failed, there is little difference in the total gas volume generated and composition.

3.1.1. The 26,650 Cell External Heat at 33, 67, and 100% SoC

The gas volumes for all the tests performed on Cell D at different SoCs and within different atmospheres are summarised in Table 5. There was no composition data collected for the air tests and 50% SoC tests.

Table 5. Gas volumes for all the external heat tests on Cell D at varying states of charge (SoCs).

Test Number	SoC (%)	Atmosphere	Maximum Temperature (°C)	Net Gas Volume Generated (L)	Net Average Gas Volume Generated (L)	Net Gas Volume (L/Ah)	Average Net Gas Volume (L/Ah)
D-1	100	Ar	374	2.9		1.0	
D-2	100	Ar	409	3.1	3.1	1.0	1.0
D-3	100	Ar	318	3.3		1.1	
D-4	67	Ar	370	2.4		1.2	
D-5	67	Ar	286	2.4	2.5	1.2	1.2
D-6	67	Ar	265	2.6		1.3	
D-7	33	Ar	213	1.6		1.6	
D-8	33	Ar	194	2.1	1.9	2.1	1.9
D-9	33	Ar	258	2.0		2.0	
D-10	100	Air	327	2.4		0.8	
D-11	100	Air	348	2.5	2.5	0.8	0.8
D-12	100	Air	333	2.7		0.9	
D-13	50	Air	261	1.9	1.9	0.8	0.8
D-14	50	N_2	215	1.9	1.9	0.8	0.8

External heat tests performed on Cell D in an open field environment showed no flames during cell failure, with only gas release observed, indicating that no flaming combustion reactions occurred (Figure 2b).

Tests in an air atmosphere showed less gas generation at 100% SoC compared to those in the Ar atmosphere. Cells at 50% SoC were observed to generate the same volume of gas regardless of the atmosphere. It should be noted that data is taken from a single data point, and no gas composition was collected for either test.

3.1.2. External Heat Gas Composition

Comparing the gas composition for cells at 33, 67, and 100% SoC under an Ar atmosphere demonstrated that the cell capacity at failure affects the final ratio. All values were averaged from three tests at each capacity. The most apparent change was in H_2 percentage volume, where at 100% SoC it accounted for 40.0% of the gas volume but decreased to 12.9% at 33% SoC. CO percentage volume remained consistent at 33 and 67% SoC, with 14.9% and 16.4%, respectively, which then decreased to 8.2% at 100% SoC. The reverse was observed for CO_2, with a 29.7% percentage volume at 33% SoC decreased to 20.0 and 16.8% at 67 and 100% SoC. This is shown in Figure 3.

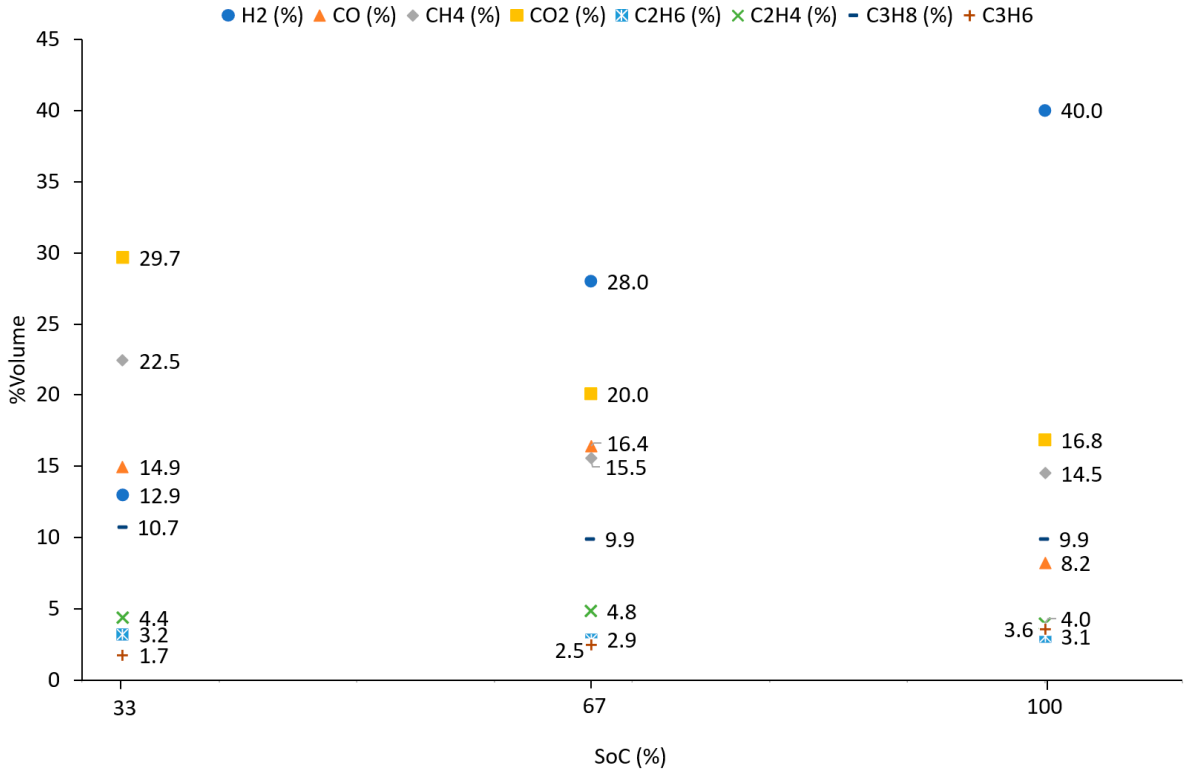

Figure 3. Average composition for H_2, CO, CO_2, CH_4, C_2H_4, C_2H_6, C_3H_6, C_3H_8 produced by failing Cell D at 33%, 67%, and 100% SoC under Ar.

CH_4 accounted for the largest percentage volume of the hydrocarbons identified, with 22.5% at 33% SoC (22.5%) before decreasing with capacity to 15.5% (67.0% SoC) and 14.5% (100% SoC). Other changes to small hydrocarbon volumes were seen for C_3H_6, with the percentage volume doubling between 33 and 100%. Finally, there was little change in the percentage volumes of C_3H_8, C_2H_6, and C_2H_4 across the capacities. The average percentage volumes for each gas at each capacity are given in Figure 3.

3.1.3. Nail Penetration Temperatures, Gas Volumes, and Composition

The nail penetration test results for Cell D showed much more variation in temperature, gas volumes, and composition compared with the external heat tests (Figure 2d). Temperature data showed differences in the maximum temperatures reached during cell failure. Cell D-15 reached the highest temperature of all three cells with a maximum recorded of 260 °C, followed by Cell D-17 at 151 °C. Cell D-16 reached a maximum temperature of 98 °C; during this test, the nail was retracted and reinserted into the cell several times to ensure failure had been reached. Each time the nail re-entered the cell, the temperature increased slightly (Figure 4).

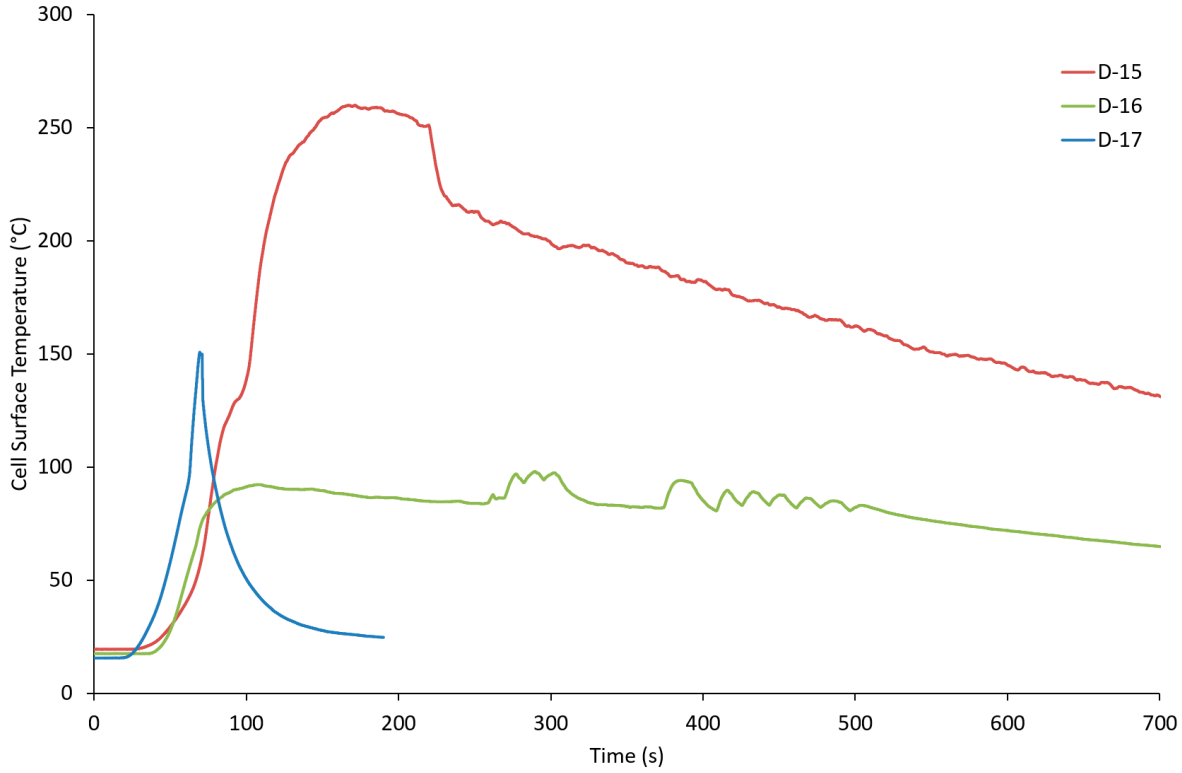

Figure 4. Temperature graphs for all three D Cells nail penetration tests, 'Cell D-15' (red), 'Cell D-16' (green), 'Cell D-17' (blue).

The different temperature profiles seen for each cell failure may have led to variations in the gas composition and volumes produced (1.0–1.9 L). The key differences in composition are seen in H_2 (6.3–46.5%) and CO (0.0–23.2%) percentage volumes. In sample D-17, where there was a CO concentration of 0%, additional analysis via Fourier Transform Infrared Spectroscopy (FTIR) was performed to corroborate these results. FTIR analysis detected a CO concentration of 12 ppm. This value (12 ppm) was also used to calculate the $v\%/v$, in addition to the mass spectrometry method, and both methods resulted in a CO percentage volume of 0.0%.

Another difference seen in the hydrocarbon percentage volumes was in CH_4 reaching a maximum of 37.6% (Cell D-16) and a minimum of 21.6% (Cell D-17). For Cell D-16, where there was an increased concentration of CH_4, a high proportion of C_3H_8 (16.3%) was recorded, over double the percentage volumes reported for the other two tests. The percentage volumes for the remaining hydrocarbons and CO_2 remained relatively consistent between tests. A summary of the gas volume and composition for each individual test is shown in Table 6.

Table 6. Net gas volume and average gas composition for all three nail penetration tests on Cell D in an inert atmosphere.

Cell ID	Net Gas Volume (L)	Net Gas Volume (L/Ah)	Gas Composition							
			H_2 (%)	CO (%)	CO_2 (%)	CH_4 (%)	C_2H_6 (%)	C_2H_4 (%)	C_3H_8 (%)	C_3H_6 (%)
D-15	1.9	0.6	22.1	23.2	14.9	22.1	3.9	5.6	7.0	1.2
D-16	1.0	0.3	6.3	13.5	17.4	37.6	1.2	4.9	16.3	2.7
D-17	1.4	0.5	46.5	0.0	15.0	21.6	4.9	4.4	6.0	1.6

The dataset demonstrates the potential for variation between nail penetration tests and highlights the importance of conducting repeat experiments using the same cell type and methodology. The failure mechanism influences the gas volume and composition, with the final values ranging between 0.3 and 0.6 L/Ah. The test results were lower compared to the external heat tests on Cell D under Ar at 100% SoC, which generated 1.0–1.1 L/Ah.

3.2. Higher Capacity Cell Results

3.2.1. External Heat Gas Volumes and Gas Composition

The cells of a higher capacity all failed via external heat using adhesive heaters stuck to the cell's surface. The size and number of heaters varied between tests due to heater availability. There was also a variation in the heater power supplied throughout the test, which in some cases was increased during the test to achieve cell failure. The exact details of the heater type, number, and power supplied are given in the supplementary data.

The gas volumes and composition generated by the higher capacity cells during failure are summarised in Table 7.

Table 7. Average net gas volumes and average gas composition for the 25 Ah pouch (Cell F), 50 Ah prismatic (Cell H), and 105 Ah prismatic (Cell J) cells failed via external heat tests under an Ar atmosphere.

Cell ID	Average Net Gas Volumes (L)	Average Gas Volume (L/Ah)	Average Gas Composition							
			H_2 (%)	CO (%)	CO_2 (%)	CH_4 (%)	C_2H_6 (%)	C_2H_4 (%)	C_3H_8 (%)	C_3H_6 (%)
Cell F (25 Ah Pouch)	15.7	0.63	48.5	7.3	14.5	5.0	3.5	10.3	6.5	4.4
Cell H (50 Ah Prismatic)	24.5	0.49	56.6	7.0	14.9	5.6	2.2	5.6	5.4	2.8
Cell J (105 Ah Prismatic)	58.1	0.55	55.1	15.2	17.4	3.7	1.2	2.8	2.9	2.3

In general, the higher capacity cells produced relatively similar gas volumes when compared as L/Ah. Results ranged from 0.49 to 0.63 L/Ah, which is comparable to 26,650 cells, Cell A and Cell B, under an inert atmosphere, but less than Cell C and Cell D. There was some variation in gas compositions, likely due to differences in electrolyte composition between manufacturers. H_2 percentage volumes were slightly higher in both prismatic cells, Cell H (56.6%) and Cell J (55.1%), compared to Cell F (48.5%). The percentage volume of CO was almost double in Cell J compared to both Cell F and Cell H, with little difference in CO_2 percentage volume across all cells. Larger differences in composition were observed when looking at hydrocarbon percentage volumes. One key difference was in the C_2H_4 percentage volume, which varied, with 2.8% produced by Cell J, 5.6% by Cell H, and 10.3% by Cell F. Other variation was seen in hydrocarbon percentage volumes, but to a lesser extent than in C_2H_4.

Images of Cell F and Cell J taken after the external heat tests can be found in Figure 2f,h.

3.2.2. Overcharge Temperature Data and Gas Volumes

The net gas volume generated by the overcharged cell and the maximum temperature reached during each test are summarised in Table 8.

Table 8. Maximum temperatures and gas volumes for the higher capacity cell overcharge tests.

Cell ID	Capacity (Ah)	Atmosphere	Max Temperature (°C)	SoC at Failure (%)	Net Gas Volume (L)	Net Gas Volume at Failure Capacity (L/Ah)	Net Gas Volume at Nominal Capacity (L/Ah)
E-1	22	Ar	225	129	19.2	0.68	0.87
E-2	22	Ar	65	129	3.2	0.11	0.15
E-3	22	Air	296	128	19.2	0.68	0.87
E-4	22	Air	94	136	3.2	0.11	0.14
G-1	32	Ar	150	129	22.2	0.54	0.69
G-2	32	Ar	63	132	20.6	0.49	0.64
I-1	50	Ar	327	149	45.5	0.61	0.91
J-4	105	Ar	526	131	77.8	0.57	0.74
J-5	105	Ar	226	-	75.9	-	0.72
K-1	230	Ar	242	125	160	0.56	0.70
K-2	230	Ar	356	123	182	0.64	0.79

Generally, the larger the cell capacity, the larger the resulting volume. However, the same trend is not observed when values are converted to L/Ah by using the cell's capacity at failure. There is little variation between cells, with typical values within a range of 0.54–0.68 L/Ah, excluding Cell E-2 and E-4. Tests performed on Cell E, one in air and one in Ar, appeared to be the exception, as the volume of gas generated was significantly lower. The significant reduction in the gas volume for Cell E-2 and E-4 may be a result of the cell not getting as hot during the test compared to the repeat tests under the same conditions (Cell E-1 and E-3). This is supported by the maximum temperature reached by Cell E-2 and E-4 being significantly lower compared to Cell E-1 and E-4, which may have affected the volume of electrolyte within the cell undergoing decomposition, therefore reducing gas volume generation. Despite this, a gas sample was able to be collected for these tests, indicating that the cells had still reached failure (Table 9).

Table 9. The average gas compositions for the higher-capacity overcharged cells. (Note: All values given are an average of two tests, except Cell I, which is taken from a single data point).

Cell ID	Capacity (Ah)	Atmosphere	Average Gas Composition							
			H_2 (%)	CO (%)	CO_2 (%)	CH_4 (%)	C_2H_6 (%)	C_2H_4 (%)	C_3H_8 (%)	C_3H_6 (%)
Cell E	22	Air	44.3	13.3	24.2	4.6	2.1	6.3	3.5	1.8
Cell E	22	Ar	42.8	17.9	21.3	3.1	1.2	7.8	2.0	4.1
Cell G	32	Ar	51.2	7.2	12.8	4.6	5.3	8.0	5.7	5.6
Cell I	50	Ar	45.3	6.0	14.0	4.8	3.8	9.7	8.4	8.0
Cell J	105	Ar	47.2	9.2	15.8	12.0	2.7	8.4	2.8	2.1
Cell K	230	Ar	33.4	18.3	22.8	6.5	3.5	11.5	2.3	1.9

3.2.3. Overcharge Gas Composition

The average gas composition for all overcharge tests on the higher capacity cells is summarised in Table 9.

Across all the cell formats tested, the cell capacity did not appear to affect the gas composition up to a cell capacity of 105 Ah. Up to a 105 Ah capacity, the highest concentration in the gas composition was H_2, which made up between 42.8 and 51.2%, followed by CO_2 (12.8–24.2%) and CO (6.0–18.3%). The 230 Ah capacity cell (Cell K) had a lower concentration of H_2 (33.4%); however, the concentration of the other gases generated by Cell K remained in a similar range when compared to the other cell types tested in this series. When comparing the gas composition for Cell E, which was tested under both an air and Ar atmosphere, there did not appear to be a significant difference in gas composition.

Comparing gas volumes between the 105 Ah prismatic (Cell J), the only cell to be failed using external heat and overcharge, shows an increased gas volume when failed via overcharge, an average of 76.9 L compared to 58.1 L when failed via external heat. This is likely to be due to an increased SoC at failure when overcharged, thereby increasing the energy density of the cell. The gas composition remains similar, with only slight differences in CO and CH_4 concentrations.

During the removal of the prismatic cells from the pressure vessel after cell failure, it was noted that some of the cell casings had swollen up during the test but remained sealed. The only visible bursting, as a result of pressure build-up, had occurred at the vent cap as per the cell design. One exception to this was one of the 230 Ah prismatic cells (Cell K), which had burst open along the top seam of the cell. During this test, a loud audible noise could be heard in the control room at the point of cell failure. A comparison of Cell J (105 Ah prismatic) and Cell K (230 Ah prismatic) after an overcharge test can be seen in Figure 5.

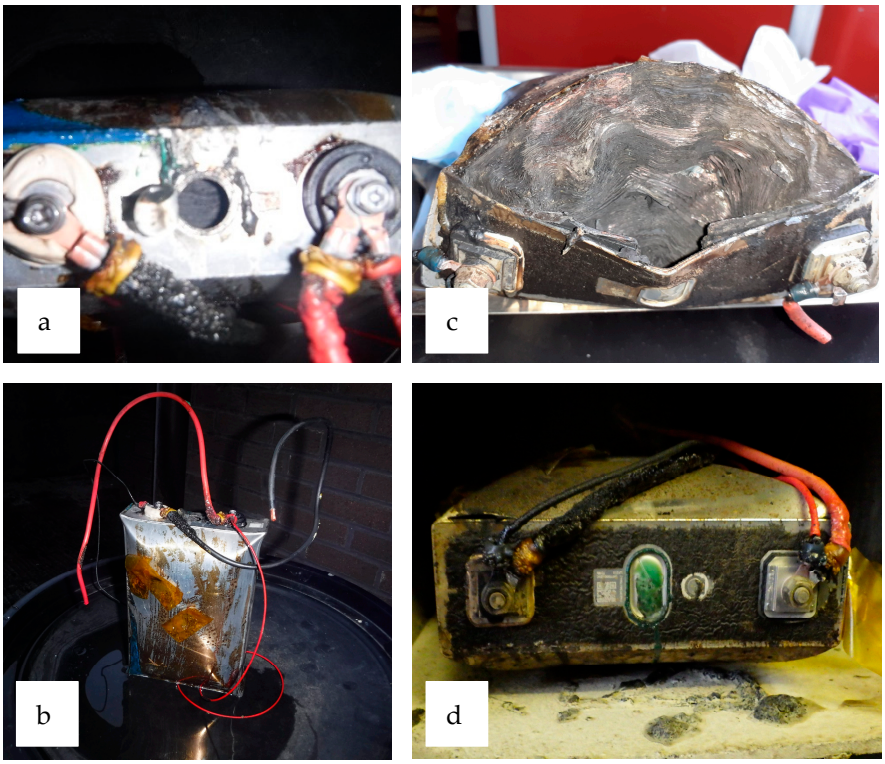

Figure 5. (**a**) Cell J vent, which burst during cell failure; (**b**) Casing of Cell J after failure, the casing had expanded but was still intact; (**c**) The casing of Cell K which had split along the seam during failure, exposing the jelly roll inside the cell; (**d**) 230 Ah cell after overcharge where the casing did not split.

3.3. Nail Penetration Open-Field Tests

In open-field tests, using nail penetration as the failure mechanism, Cells F, H, and J did not reach failure. Video footage of the tests did not indicate signs of failure, e.g., smoke, gas, sparks, or flame, and there was no visible damage to the cell after the test except the puncture mark from the nail. Throughout all open-field nail penetration tests, multiple type-K thermocouples were attached to the cell's surface.

3.3.1. Cell F (25 Ah Pouch) Temperature Data

Temperature data was recorded using type-K thermocouples attached in the centre of the cell on the front and back surfaces. A slight temperature increase was recorded for the

25 Ah pouch cell with the front thermocouple reaching 19 °C and the back thermocouple reaching 19 °C before cooling back down (Figure 2j).

3.3.2. Cell H (50 Ah Prismatic) Temperature Data

For the prismatic cell, a slight temperature increase was observed when the nail entered the cell, which was picked up by all eight thermocouples; however, this soon began to decrease. The maximum temperature recorded was 21 °C, picked up by a type-K thermocouple attached to the bottom right corner of the cell's surface (Figure 2i).

3.3.3. 105 Ah (Cell J) Prismatic Temperature Data

During the main part of the test, a slow increase in temperature was observed by both thermocouples, reaching approximately 37 °C before plateauing. The cell was left in the test chamber with the data recording at a slower rate of 10 s. During this time, the temperature in front of the nail and behind the nail reached maximums of 45 and 46 °C, respectively, before beginning to cool.

Due to the lack of obvious failure during open-field nail penetration tests, these were not performed in the pressure vessel.

The temperature data recorded for all three open-field nail penetration tests are shown in Figure 6.

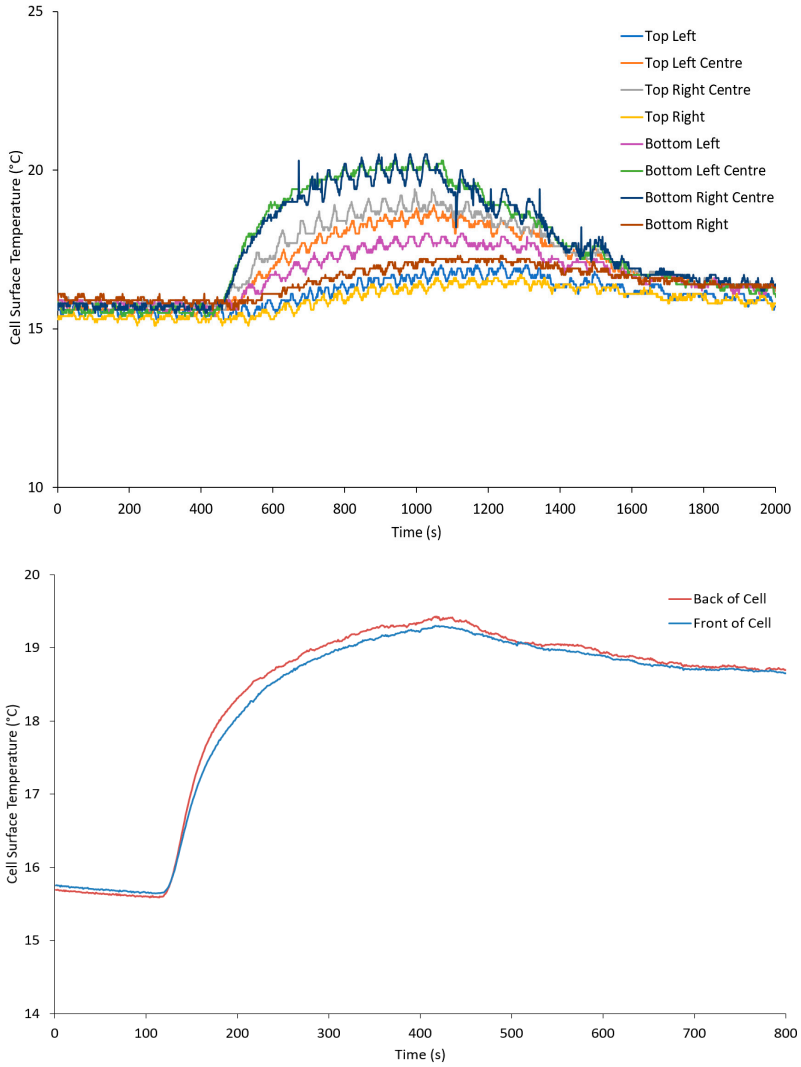

Figure 6. *Cont.*

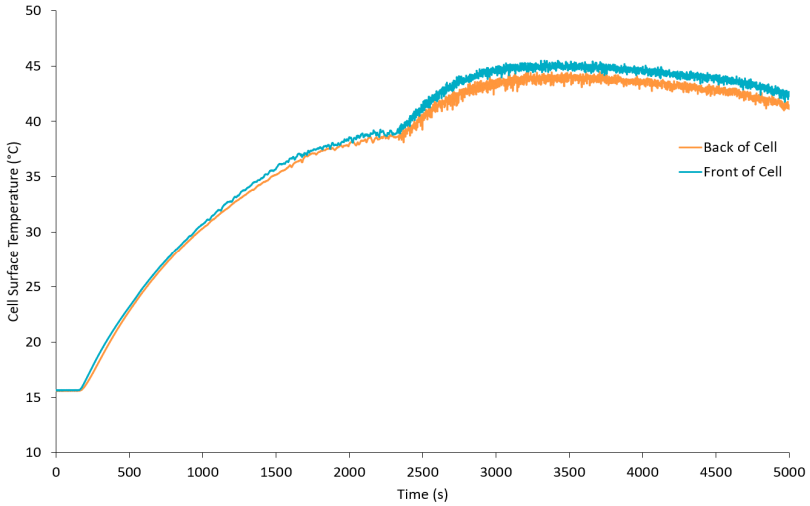

Figure 6. Temperature graph for open-field nail penetration test on the 50 Ah prismatic (Cell H) (**top**), 25 Ah pouch (Cell F) (**middle**), and 105 Ah prismatic (Cell J) (**bottom**) (Note: For the test on the 105 Ah the switch from recording the standard test data (1 s) is marked in red).

4. Conclusions

Data for the wide range of LFP cells tested indicated that the abuse method and SoC can affect the gas volume and composition generated by cells during failure. Typically, when cells failed via external heat under an inert atmosphere at a 100% SoC, approximately 0.8 L/Ah of gas is generated. The gas generated consists of approximately 40% H_2, CO_2, and CO, with the rest made up of various flammable hydrocarbons, in varying concentrations. The volume of gas is also shown to increase with the cell's SoC; however, when calculated as a gas volume in L/Ah, it remains consistent.

The abuse method is also shown to have an effect, as nail penetration tests found that less than 0.5 L/Ah of gas is generated during failure, which is much less than in external heat tests. There was also a slight decrease in gas volume generation in overcharge compared to external heat tests, typically generating 0.6 L/Ah. The gas composition, however, was like that of the external heat tests, with H_2 contributing to between 40 and 50% of the gas sample, CO_2 contributing 25%, and the rest containing varying levels of CO and hydrocarbons.

Supplementary Materials: The following supporting information can be downloaded at: https://www.mdpi.com/article/10.3390/batteries11070267/s1, Table S1—Data collected from all external heat tests; Table S2—Data collected from all overcharge tests; Table S3—Data from all nail penetration tests performed; Table S4—Test details including number of heaters, heater type, and the heater power supplied for the higher capacity external heat tests.

Author Contributions: G.E.H.: Conceptualisation, Formal Analysis, Investigation, Visualisation, Writing—original draft. J.E.H.B.: Conceptualisation, Funding Acquisition, Supervision, Writing—review and editing. J.G.: Conceptualisation, Funding Acquisition, Supervision, Writing—review and editing. S.L.G.: Data Curation, Formal Analysis, Investigation, Methodology, Validation. J.W.M.: Investigation. P.A.P.R.: Formal Analysis, Investigation. All authors have read and agreed to the published version of the manuscript.

Funding: This work was funded by the Health and Safety Executive, UK.

Data Availability Statement: The data presented in this study are available in the article and supplementary data.

Conflicts of Interest: The authors declare that they have no known competing financial interests or personal relationships that could have appeared to influence the work reported in this paper.

Abbreviations

LFP	Lithium iron phosphate
SoC	State of charge
LIB	Lithium-ion batteries
EV	Electric vehicles
TR	Thermal runaway
SATP	Standard atmospheric temperature and pressure
SEI	Solid electrolyte interphase
IR	Internal resistance
CCCV	Constant current constant voltage
EIS	Electrochemical impedance spectroscopy
ACIR	Alternating current internal resistance
FTIR	Fourier Transform Infrared Spectroscopy

References

1. Department for Buisness and Trade. *UK Battery Strategy*; Department for Business and Trade: London, UK, 2023.
2. Clemens, K. Tesla Kicks Off Future of LFP Batteries in EVs. Available online: https://eepower.com/tech-insights/tesla-kicks-off-future-of-lfp-batteries-in-evs/#:~:text=Tesla%E2%80%99s%20decision%20to%20use%20LFP%20in%20its%20Semi,significantly%20longer%20than%20those%20equipped%20with%20nickel%20cathodes (accessed on 22 October 2024).
3. Johnson, P. BYD is Launching its Next-Gen Blade EV Battery Soon with More Range and Even Lower Cost. Available online: https://electrek.co/2024/04/08/byd-launch-next-gen-ev-battery-more-range-lower-price/ (accessed on 7 November 2024).
4. Bugryniec, P.J.; Davidson, J.N.; Cumming, D.J.; Brown, S.F. Pursuing safer batteries: Thermal abuse of $LiFePO_4$ cells. *J. Power Sources* **2019**, *414*, 557–568. [CrossRef]
5. Feng, X.; Ouyang, M.; Liu, X.; Lu, L.; Xia, Y.; He, X. Thermal runaway mechanism of lithium ion battery for electric vehicles: A review. *Energy Storage Mater.* **2018**, *10*, 246–267. [CrossRef]
6. Golubkov, A.W.; Fuchs, D.; Wagner, J.; Wiltsche, H.; Stangl, C.; Fauler, G.; Voitic, G.; Thaler, A.; Hacker, V. Thermal-runaway experiments on consumer Li-ion batteries with metal-oxide and olivin-type cathodes. *RSC Adv.* **2014**, *4*, 3633–3642. [CrossRef]
7. Huang, Z.; Li, X.; Wang, Q.; Duan, Q.; Li, Y.; Li, L.; Wang, Q. Experimental investigation on thermal runaway propagation of large format lithium ion battery modules with two cathodes. *Int. J. Heat Mass Transf.* **2021**, *172*, 121077. [CrossRef]
8. Mao, B.; Ma, Y.; Zhang, K.; Li, X.; Lu, J.; Zhang, Y.; Wen, J.X. Self-ignition, jet flame and thermal radiation hazards associated with the large-size $LiFePO_4$ cell during thermal runaway. *J. Power Sources* **2024**, *622*, 253361. [CrossRef]
9. Golubkov, A.W.; Scheikl, S.; Planteu, R.; Voitic, G.; Wiltsche, H.; Stangl, C.; Fauler, G.; Thaler, A.; Hacker, V. Thermal runaway of commercial 18650 Li-ion batteries with LFP and NCA cathodes: Impact of state of charge and overcharge. *RSC Adv.* **2015**, *5*, 57171–57186. [CrossRef]
10. Yuan, L.; Dubaniewicz, T.; Zlochower, I.; Thomas, R.; Rayyan, N. Experimental study on thermal runaway and vented gases of lithium-ion cells. *Process Saf. Environ. Prot.* **2020**, *144*, 186–192. [CrossRef]
11. Sturk, D.; Rosell, L.; Blomqvist, P.; Tidblad, A.A. Analysis of Li-Ion Battery Gases Vented in an Inert Atmosphere Thermal Test Chamber. *Batteries* **2019**, *5*, 61. [CrossRef]
12. Yang, M.; Rong, M.; Pan, J.; Ye, Y.; Yang, A.; Chu, J.; Yuan, H.; Wang, X. Thermal runaway behavior analysis during overheating for commercial $LiFePO_4$ batteries under various state of charges. *Appl. Therm. Eng.* **2023**, *230*, 120816. [CrossRef]
13. Wang, H.; Xu, H.; Zhang, Z.; Wang, Q.; Jin, C.; Wu, C.; Xu, C.; Hao, J.; Sun, L.; Du, Z.; et al. Fire and explosion characteristics of vent gas from lithium-ion batteries after thermal runaway: A comparative study. *eTransportation* **2022**, *13*, 100190. [CrossRef]
14. Yang, X.; Wang, H.; Li, M.; Li, Y.; Li, C.; Zhang, Y.; Chen, S.; Shen, H.; Qian, F.; Feng, X.; et al. Experimental Study on Thermal Runaway Behavior of Lithium-Ion Battery and Analysis of Combustible Limit of Gas Production. *Batteries* **2022**, *8*, 250. [CrossRef]
15. Shen, H.; Wang, H.; Li, M.; Li, C.; Zhang, Y.; Li, Y.; Yang, X.; Yang, X.; Feng, X.; Ouyang, M. Thermal Runaway Characteristics and Gas Composition Analysis of Lithium-Ion Batteries with Different LFP and NCM Cathode Materials Under Inert Atmosphere. *Electronics* **2023**, *12*, 1603. [CrossRef]
16. Yang, M.; Rong, M.; Ye, Y.; Yang, A.; Chu, J.; Yuan, H.; Wang, X. Comprehensive analysis of gas production for commercial $LiFePO_4$ batteries during overcharge-thermal runaway. *J. Energy Storage* **2023**, *72*, 108323. [CrossRef]
17. Fernandes, Y.; Bry, A.; De Persis, S. Identification and quantification of gases emitted during abuse tests by overcharge of a commercial Li-ion battery. *J. Power Sources* **2018**, *389*, 106–119. [CrossRef]
18. Wang, H.; Wang, Q.; Jin, C.; Xu, C.; Zhao, Y.; Li, Y.; Zhong, C.; Feng, X. Detailed characterization of particle emissions due to thermal failure of batteries with different cathodes. *J. Hazard. Mater.* **2023**, *458*, 131646. [CrossRef] [PubMed]

19. Said, A.O.; Lee, C.; Stoliarov, S.I. Experimental investigation of cascading failure in 18650 lithium ion cell arrays: Impact of cathode chemistry. *J. Power Sources* **2020**, *445*, 227347. [CrossRef]
20. Peng, Y.; Yang, L.; Ju, X.; Liao, B.; Ye, K.; Li, L.; Cao, B.; Ni, Y. A comprehensive investigation on the thermal and toxic hazards of large format lithium-ion batteries with $LiFePO_4$ cathode. *J. Hazard. Mater.* **2020**, *381*, 120916. [CrossRef] [PubMed]
21. Abbott, K.C.; Buston, J.E.H.; Gill, J.; Goddard, S.L.; Howard, D.; Howard, G.; Read, E.; Williams, R.C.E. Comprehensive gas analysis of a 21700 Li ($Ni_{0.8}Co_{0.1}Mn_{0.1}O_2$) cell using mass spectrometry. *J. Power Sources* **2022**, *539*, 231585. [CrossRef]
22. Howard, G.; Buston, J.; Gill, J. Experimental understanding of gas volumes and forces generated due to swelling during lithium-ion pouch cell failure. In Proceedings of the Hazards 31, Virtual, 16–18 November 2021.
23. Howard, G.E.; Abbott, K.C.; Buston, J.E.H.; Gill, J.; Goddard, S.L.; Howard, D. Comprehensive Study of the Gas Volume and Composition Generated by 5 Ah Nickel Manganese Cobalt Oxide (NMC) Li-Ion Pouch Cells Through Different Failure Mechanisms at Varying States of Charge. *Batteries* **2025**, *11*, 197. [CrossRef]
24. Chen, S.; Wang, Z.; Yan, W. Identification and characteristic analysis of powder ejected from a lithium ion battery during thermal runaway at elevated temperatures. *J. Hazard. Mater.* **2020**, *400*, 123169. [CrossRef] [PubMed]